



CrossMark
 click for updates

Cite this: *RSC Adv.*, 2015, 5, 106128

Ammonolysis of gallium phosphide GaP to the nanocrystalline wide bandgap semiconductor gallium nitride GaN

Mariusz Drygas,^a Maciej Sitarz^b and Jerzy F. Janik^{*a}

The pnictogen-metathesis reaction of microcrystalline gallium phosphide GaP with ammonia NH₃ at temperatures of 900–1150 °C for 6–60 hours afforded in one step nanocrystalline powders of the wide bandgap semiconductor gallium nitride GaN. A suitable choice of conditions including variations of reaction temperature/time and manual grinding or high energy ball milling of the substrate enabled control over distinct GaN particle morphologies, regularly shaped particles or nanowires, and average crystallite sizes up to a few tens of nanometers. Under the applied conditions, all by-products were conveniently removed as volatiles affording pure GaN nanopowders. In contrast to ammonolysis of the related cubic GaAs and cubic GaSb, which yielded mixtures of the hexagonal and cubic GaN polytypes, here, the nitride was made exclusively as the stable hexagonal variety. All this supported specific reaction pathways with thermodynamics solely controlling the ammonolytical conversion of the cubic GaP substrate to the hexagonal GaN product.

Received 3rd November 2015

Accepted 1st December 2015

DOI: 10.1039/c5ra23144b

www.rsc.org/advances

1. Introduction

Gallium nitride GaN has burst into modern electronics thanks to its unique pool of properties notably including the wide badgap of 3.4 eV for hexagonal GaN or 3.2 eV for cubic GaN, both suitable for diverse optoelectronic applications. It is worth underlining gallium nitride's feasibility to make solid solutions with other Group III(13)-nitrides, which in the form of thin films nowadays constitute the basis for pivotal light-emitting diodes and lasers in the ultraviolet and visible blue ranges.^{1,2} Additionally, theoretical and practical capacities of nitride's lattice, which can be modified with suitable centers, create conditions for effective modifications of the material's semi-conducting, optical, and magnetic properties at once.^{1e,3} To this point, numerous methods reported for the synthesis of GaN prevaillingly address the GaN-based thin film formation and/or making monocrystalline GaN optoelectronic device supports. At the same time, the progress in developing convenient and high-yield synthesis methods for GaN nanopowders is not yet satisfactory as exemplified by some of the reviews on the subject.⁴ The available methods are mostly based on utilization of the affordable gallium metal or gallium oxygen-bearing precursors in reactions with a nitrating agent such as ammonia or nitrogen whereas, sometimes, selected organo-metallic gallium precursors have also been tried.

Some of us contributed to developing a number of new synthesis routes to GaN nanopowders such as the metathesis in the system GaX₃/Li₃N (X = Cl, Br),⁵ original preparation and deamination of polymeric gallium imide {Ga[NH]_{3/2}}_n⁶ and cyclotrigalazane [H₂GaNH₂]₃⁷ as well as the ammonolysis of readily available gallium nitrate aerosolized solutions.^{6g-i,8} Based on this experience, we can stress the advantages of both the anaerobic gallium imide route, which yields average crystallite sizes of oxygen-free GaN ranging from one to several tens of nanometers and the aerosol-assisted method, which uses the affordable gallium nitrate precursor in a relatively large-scale synthesis. However, the gallium imide route is a multi-stage method that requires elaborate equipment and complex processing characteristic of anaerobic syntheses. Along this way, the aerosol-assisted route is a two-step synthesis resulting in rather large average crystallite sizes above 30 nm with intrinsic chances of getting residual oxygen in the product. Actually, we are not aware of a method that would economically supply large quantities of pure, size and polytype-controlled nanopowders of GaN. This aspect has become a real problem in our otherwise successful trials of high-temperature high-pressure sintering of GaN nanopowders into robust ceramics.⁹ We directly learned that an economical and well-controlled method of GaN nanopowder synthesis has yet to be worked out.

For reaching such a goal, we have focused our efforts on metathetical ammonolysis of such gallium pnictides as GaAs, GaSb, and GaP which, in principle, should yield GaN in one step and high yields. The large scale preparation of these gallium pnictides as bulk crystals, the valuable semiconductors, is well developed *via* the Czochralski method and, additionally,

^aAGH University of Science and Technology, Faculty of Energy and Fuels, al. Mickiewicza 30, 30-059 Krakow, Poland. E-mail: janikj@agh.edu.pl

^bAGH University of Science and Technology, Faculty of Materials Science and Ceramics, al. Mickiewicza 30, 30-059 Krakow, Poland

considerable quantities of the materials seem to be available as post-processing wastes in electronic industry. First, we re-examined the known reaction of cubic gallium arsenide GaAs with ammonia which yielded increased proportions of the rare cubic gallium nitride, c-GaN.^{10a-c} We showed that up to some 90% of c-GaN could be prepared in admixture with the hexagonal polytype, h-GaN. It is appropriate to mention that c-GaN is thermodynamically a metastable phase, thus, its prevailing formation can be linked to advantageous topochemical circumstances during ammonolysis with N for As replacements in the cubic lattice of the GaAs substrate. Second, we have recently explored a related system GaSb/NH₃, which afforded definite mixtures of both GaN polytypes, this time with the increased amounts of h-GaN in the 66–92% range.^{10d} It appeared for these two systems, that a fine interplay of the thermodynamic and topochemical/kinetic factors determined the GaN polytype make-up. In this regard, the evolution of particle size/surface during substrate grinding was found essential in deciding which of the factors was dominant. For instance, the ball milled GaSb powders resulted consistently in GaN nanopowders with the very much constant 66–68% contents of h-GaN for a range of applied conditions suppressing to a great extent the temperature/time effect. The resulting GaN nanopowders were shown to be of very good quality including high purity and structural integrity.

In continuation of the project, herein, described is the synthesis of nanocrystalline GaN by ammonolysis of microcrystalline gallium phosphide GaP. Given the standard enthalpies of formation for GaP (−25 kJ mol^{−1}), NH₃ (−46 kJ mol^{−1}), GaN (−157 kJ mol^{−1}), and PH₃ (−5 or −23 kJ mol^{−1}, depending on the white P or red P reference state, respectively), the standard reaction enthalpy for a model metathesis reaction of the type GaP + NH₃ → GaN + PH₃ is negative and, therefore, thermodynamically supported. Taking into account the various mixtures of the GaN polytypes formed in the related GaAs/NH₃ and GaSb/NH₃ systems, a potential significance of topochemistry in shaping up reaction outcome in the GaP/NH₃ system has had to be experimentally appraised. Specifically, in this project monocrystalline chunks of GaP were either manually ground in an agate mortar or milled in a high energy ball mill, which was followed by pyrolysis under a flow of ammonia for up to 150 hours at temperatures in the range 800–1200 °C. The products were yellowish to gray yellowish, loosely agglomerated powders that were extensively characterized.

2. Experimental

2.1. Synthesis

Chunks of GaP of commercial quality were acquired as waste material from the Institute of Electronic Materials Technology, Warszawa, Poland. The material required grinding that was accomplished with two different methods. In manual grinding, a few grams of dark yellow-brownish chunks were placed in an agate mortar and ground for approximately 10 minutes to afford a dark yellowish powder. For deep grinding by wet high energy ball milling, a few grams of chunks crashed to sizes below ca. 1 mm were placed in a grinding bowl of the FRITSCH

Pulverisette 7 planetary ball mill onto which 10 ml of dry xylene were added. Twenty 3 minute intermittent grinding periods were applied at 900 rpm, each separated by a 10 minute break to prevent overheating of the bowl's content. After each grinding period, the bowl warmed up to 50–60 °C much below the boiling point of xylene, 140 °C. Following recovery from the bowl, the sticky paste was evacuated for 1 h to remove volatiles affording a slightly agglomerated precursor powder. A sample of dry ball milled GaP was also prepared by the identical procedure carried out without xylene. A batch of 1 to 2 grams of the powder was placed in an alumina boat and inserted into a ceramic reactor in a tube furnace. Prior to heating, the system was purged with high purity ammonia, 99.999%, 30 min, 0.05 L min^{−1}, and such a flow rate was maintained throughout the reaction. A selected reaction temperature was attained with a heating rate of 5 °C min^{−1}. Preliminary experiments were carried out at 800 and 850 °C for up to 150 hours to afford mixtures of unconverted GaP and some GaN. For the reaction at 900 °C, hold times in the range of 36–60 hours resulted in complete nitridation. For the reactions at 1000–1150 °C, a 6 to 36 hour heating time accomplished the same goal. An additional single experiment at 1200 °C, 12 hours, resulted in complete decomposition of GaN towards volatile species producing an empty crucible. The reactions were carried out for both the manually ground and ball milled GaP powders. Upon cooling to room temperature under flowing ammonia, each sample was evacuated for 30 minutes to remove volatiles. The final products were gray yellowish, loosely agglomerated powders.

2.2. Characterization

Particle size distribution for substrate powders was measured by dynamic light scattering on Nanosizer-ZS of Malvern Instruments. All substrates and products were characterized by standard powder XRD analysis (X'Pert Pro Panalytical, Cu K_α source; 2θ = 10–110°). Average crystallite sizes were evaluated from Scherrer's equation applying the Rietveld refinement method. For the evaluation, changes of the line profile parameters compared to a standard sample were utilized. The profile parameters depend on the instrument settings used for data collection and on the profile function used for the refinement. In our analysis, the full Voigt function was used to describe the profile of the measured diffraction lines. The total profile width is a convolution of the Gaussian profile part and of the Lorentzian profile part and these parts are combined numerically. In such a method, the full width at half-maximum (fwhm) is only one of several fitted parameters. Solid-state ⁷¹Ga MAS NMR spectra were acquired on the APOLLO console (Tecmag) at the magnetic field of 7.05 T produced by a 89 mm bore superconducting magnet (Magnex). A Bruker HP-WB high-speed MAS probe equipped with a 4 mm zirconia rotor and KEL-F cap was used to record the MAS NMR spectra at the spinning rates of 6 or 8 kHz. The resonance frequency was equal to 91.385 MHz and a single 2 μs rf pulse was used, which corresponded to π/4 flip angle in the liquid. The acquisition delay used in accumulation was 1 second and the typical number of acquisitions ranged from 1000 to 4000. The frequency scale in ppm was referenced

to Ga(NO₃)₃ (1 M in D₂O). All resonance positions were uncorrected for the second-order quadrupolar shift. Micro-Raman analysis was generally done by HORIBA LabRAM HR spectrometer with 532 nm laser, sample power of 20 mW, accumulation time 10 s and 2 scans, confocal hole 1000 μm with long-focus length. For two samples showing strong non-specific luminescence, which could not be measured with the 532 nm laser, a laser operating at 325 nm, sample power of 10 mW, accumulation time 10 s and 2 scans, and confocal hole 1000 μm with long-focus length was used; however, due to instrumental artefacts this limited the lowest shift to be at 400 cm⁻¹. UV-vis data were collected on a Perkin-Elmer spectrophotometer Lambda 35 equipped with a 50 mm integrating sphere. SEM/EDX data were acquired with a Hitachi Model S-4700 scanning electron microscope.

3. Results and discussion

3.1. Chemistry and thermodynamics in the system

The anticipated chemistry behind the metathetical nitridation of GaP can be summarized by a thermodynamically supported simplified reaction of the type GaP + NH₃ → GaN + PH₃ paralleling the related systems of GaAs/NH₃^{10c} and GaSb/NH₃.^{10d}

Phosphine PH₃ is a gas stable at ambient conditions (ΔH_f° PH₃ = -5 or -23 kJ mol⁻¹) and known to decompose into several species including P₂ and P₄ vapors at increased temperatures, especially, higher than 550–600 °C.¹¹ Under the currently applied conditions, one could therefore expect condensation of the by-product vapors into red and/or white phosphorus in colder parts of the set-up^{11d} leaving a pure GaN product in the hot zone with no separation efforts. In no case, any phosphorus was detected by XRD in the products. Also, all completely reacted nanopowders were examined by SEM/EDX to show no P within the method detection limits.

It is worth to note that at temperatures in the range 900–1150 °C the GaP substrate is potentially to undergo some decomposition into liquid gallium metal (mp 30 °C) and phosphorus vapors. As the matter of fact, solid GaP is reported to evaporate congruently only up to ca. 680 °C^{12a} to show at the melting point of 1520 °C a dissociation pressure of 35 atm.^{12b} Despite this, ball milled powders of GaP have seemed to be successfully applied to make GaP nanowires in the temperature range 950/1100 °C under argon *via* “sublimation” method.^{12c} At the same time, the propensity of GaP to vaporize incongruently has been utilized in constructing devices with GaP decomposition-derived P-sources for molecular beam epitaxy.¹³ Thus, on the one hand, the relatively low decomposition temperatures of GaP may create a situation of ammonia reacting with isolated gallium droplets towards GaN after all. On the other hand, if conditions for significant GaP evaporation exist, *e.g.*, by virtue of increased particle surface area upon deep grinding by ball milling, gas phase reactions between the sublimed GaP species and ammonia may come to play. For both reactions outlined above, the thermodynamically favored hexagonal polytype of GaN is expected to form nonetheless of distinct habits.

The known chemistry of GaP towards nitrogen sources is rather scarce with a notable exception of N-doping of various

GaP structures including nanowires for electronic applications.¹⁴ As the matter of fact, N-incorporation into cubic GaP made at some point possible the commercial production of yellow light-emitting sources.¹⁵ A singular report on the stability of GaP nanopowders under nitrogen determined an unexpected formation of the metastable cubic GaN, sometimes admixed with elemental Ga, upon treatment at 500 °C.¹⁶ In our opinion, the authors rather incorrectly proposed a reaction mechanism involving a decomposition of GaP to the elemental Ga and P followed by reactions of Ga with N₂ particles to form GaN. Even if it is only hardly possible that nanodroplets of Ga could react with molecular nitrogen towards gallium nitride under such conditions, it is very unlikely to expect from it the metastable c-GaN after all. It is rather a gradual and topochemically controlled replacement of P with N in the cubic lattice of nanosized GaP that offers plausible explanation of c-GaN formation. In line of “unexpected” outcomes concerned with the related chemistry of GaP, another report described the preparation of N-doped single crystalline GaP nanowires by sublimation of ball milled GaP powders under an ammonia flow in the temperature range 950 (substrate)–1100 °C (source).^{14a} A merely moderate N-doping of the resultant cubic GaP nanowires at the level of ca. 10¹⁸ cm⁻³ was estimated whereas there was no evidence for nitridation towards GaN. This certainly seems to be very much in contradiction to the anticipated chemistry of our project that is nevertheless firmly rooted in the confirmed nitridation chemistry in the related systems of GaAs/NH₃ and GaSb/NH₃.

When looking at stabilities of the two most common GaN polytypes, theoretical calculations suggest a very small difference in standard total energies between the hexagonal (wurtzite) and cubic (zinc blende) polytypes.¹⁷ The total energy of c-GaN is lower merely by 9.88 meV per atom or 16 meV per unit compared with that of h-GaN which implies that the formation of the nitride's metastable cubic phase is practically possible and may depend on the choice of specific reaction/experimental conditions (kinetic control, extreme pressure/temperature, substrate surface-nitride layer lattice compatibility, topochemistry). In this regard, there are known reports confirming the preparation of pure c-GaN, mostly, as thin films¹⁸ or polycrystalline products from autoclave syntheses^{9f,19} whereas under moderate conditions the c-GaN is often accompanied by the stable h-GaN in physical mixtures of the polytypes but, also, *via* stacking faults in multidomain nanostructures.²⁰ All this points out to, merely, a complementary role of thermodynamics in controlling GaN polytype formation in many precursor systems and is well exemplified by the diverse phase mixtures of the nitride formed in the systems of GaAs/NH₃ and GaSb/NH₃.

One could suppose that under appropriate conditions the P-centers in the cubic GaP would be suitably replaced with the N-centers from ammonia decomposition preserving the cubic lattice, first, in the form of transient c-GaPN and, eventually, producing the metastable c-GaN. Such a transitional conversion of c-GaP to c-GaN *via* a gradually collapsing cubic lattice is appealing since their respective *a* lattice constants, 5.45 and 4.50 Å, differ significantly to favor up front the lattice type preservation. It is appropriate to recall again that the

metathetical N-center mediated replacement was effective to varying degrees in the systems GaAs/NH₃ and GaSb/NH₃. However, if thermodynamics prevails the stable h-GaN will be formed, instead.²¹ As already mentioned, the latter scenario is likely to take place if GaP is preferentially decomposed to elements before metathetically reacting with NH₃ and the resulting liquid gallium is then nitrated towards GaN. However, a plausible competing sublimation of GaP can open another pathway to GaP + NH₃ reactions in the gas phase with specific product morphologies nevertheless with thermodynamically driven formation of the exclusive hexagonal polytype of GaN. From this viewpoint, other factors kept in proportion, the grain/surface size of the powdered GaP precursor can be expected to greatly impact product morphology.

3.2. Discussion of characterization data

Fig. 1 shows three particle size distribution curves – one for manually ground and two for high energy ball milled GaP, the latter including the dry and wet milling conditions. An approximately trimodal size distribution characteristics of all curves is apparent with the upper *ca.* 100–200 μm particle size limit. Each size mode differs from neighboring by, roughly, one order of magnitude. For manual grinding, the most abundant particle size range is around 100 μm and this quite a narrow mode becomes weaker for dry ball milling and persists as residual for wet ball milling. The second and broader mode encompasses particles peaking in the 10–20 μm size range. The third and equally broad mode is located in the 0.5–0.8 μm size range. This mode is only residual for the manually ground GaP but dominates in the wet ball milled GaP. It is worth noticing the distinctly different character of the distribution curves for the two ways of ball milling with wet milling providing on average much smaller and more size homogeneous particles. Although not obvious from the curves which have, practically, the particle size range limits of 0.1–2000 μm, ball milling causes a noticeable amorphization of crystallites in the low nanosized range as detected by XRD (*vide infra*). Also, it is typical for dry ball milling to result in small quantities of surface-pulverized tungsten carbide WC from grinding balls. In order to remedy this problem, a wet ball milling is applied whereas in the presence of a suitable liquid the attrition is usually minimized beyond detection. However, for very hard materials this may not work efficiently. In our experience, the wet ball milling of gallium antimonide meets fully the expectations (close to monomodal size distributions, small particle sizes, no WC attrition)^{10d} whereas gallium phosphide appears to be much harder (trimodal size distributions, larger particle sizes) and some WC wear off is expected.

The selected representative XRD patterns for nanopowders are shown in Fig. 2–4 and the calculated structural parameters, relative amounts of phases, and average particle sizes for all measured samples are included in Table 1.

The manually ground GaP shows a XRD pattern matching the reference data for bulk GaP (JCPDS no. 12-0191) (Fig. 2). The pattern for the dry ball milled phosphide is visibly broadened indicating a degree of sample amorphization. Actually, the

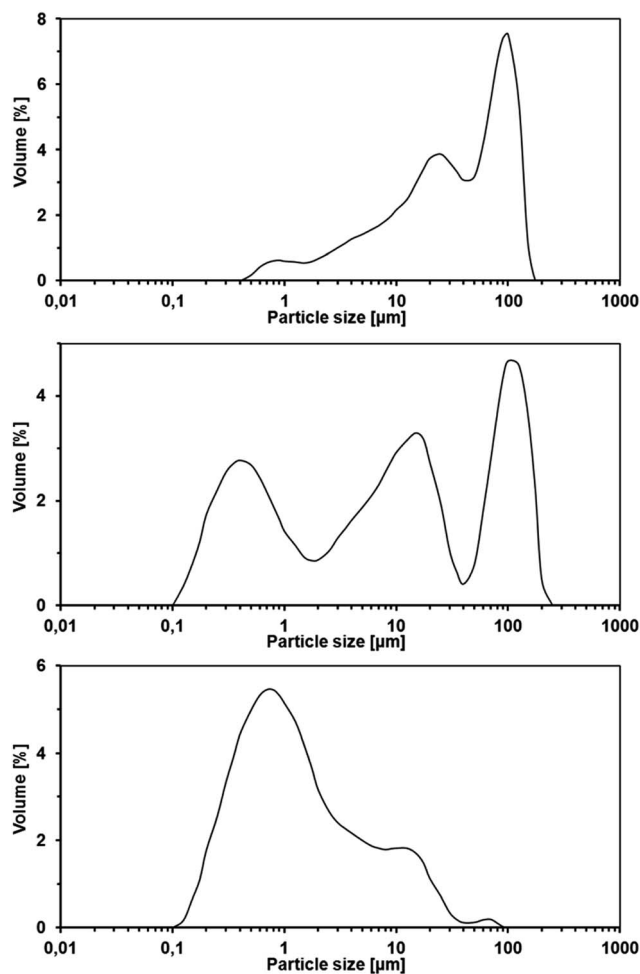


Fig. 1 Particle size distribution curves of ground GaP: top – manually ground, middle – dry ball milled, bottom – wet ball milled.

pattern can be satisfactorily deconvoluted by assuming, in addition to the major microcrystalline component, two formal particle size fractions in the low nanometer range, 9 and 31 nm (Table 1). The dry milling results also in a small content of the grinding ball-originated WC component. There is no doubt that ball milling yielded a substrate powder with an increased surface area compared with manual grinding.

The XRD pattern for the powder from the 850 °C, 90 h-conversion of the manually ground GaP supports only a partial nitridation with *ca.* 26% of h-GaN (JCPDS no. 50-0792) and the remaining of unreacted GaP, the latter with much smaller average crystallite sizes than the starting substrate (Fig. 3, left). No other phases are detected. The average crystallite size *D* for h-GaN is estimated at 18 nm. A typical pattern for a completely nitrated sample is shown for the 900 °C, 60 h-conversion in Fig. 3, right. The only crystalline component is satisfactorily indexed as h-GaN with *D* equal 19 nm. For all other nanopowders prepared from the manually ground GaP similar XRD patterns were recorded and the calculated parameters for the exclusive h-GaN product are included in Table 1. For well crystalline samples, additionally, crystallite sizes *D* along the low angle plane directions in h-GaN, *i.e.*, (100), (002), (101), were

Table 1 Amounts and structural parameters of reference and product powders. MG – manual grinding, DBM – dry ball milling, WBM – wet ball milling, n/d – not determined

| Powder (temperature, time/grinding) | Phase, content [%] | Lattice parameters a [Å], c [Å] | Av. crystallite size D (range of D) [nm] |
|-------------------------------------|-------------------------------------|--|---|
| Reference GaP/MG | c-GaP, 100 | $a = 5.45$ | >200 |
| Reference GaP/DBM | c-GaP small, 60 | $a = 5.45$ | 9 |
| | c-GaP large, 35 | $a = 5.46$ | 31 |
| | WC, 5 | n/d | n/d |
| 800 °C, 90 h/MG | c-GaP, 86 | $a = 5.45$ | 56 |
| | h-GaN, 14 | $a = 3.14$ | 18 |
| | | $c = 5.12$ | |
| 850 °C, 90 h/MG | c-GaP, 74 | $a = 5.45$ | 86 |
| | h-GaN, 26 | $a = 3.14$ | 22 |
| | | $c = 5.10$ | |
| 850 °C, 150 h/DBM | c-GaP, 27 | $a = 5.45$ | 49 |
| | h-GaN, 67 | $a = 3.15$ | 13 |
| | | $c = 5.14$ | |
| | h-WC, 6 | n/d | n/d |
| 900 °C, 36 h/MG | c-GaP, 3 | $a = 5.46$ | 47 |
| | h-GaN, 97 | $a = 3.15$ | 10 (9–11) |
| | | $c = 5.15$ | |
| 900 °C, 60 h/MG | h-GaN, 100 | $a = 3.16$ | 13 (12–15) |
| | | $c = 5.15$ | |
| 900 °C, 90 h/MG | h-GaN, 100 | $a = 3.18$ | 19 (19–20) |
| | | $c = 5.18$ | |
| 900 °C, 36 h/DBM | h-GaN, 94 | $a = 3.17$ | 16 (15–16) |
| | | $c = 5.17$ | |
| | h-WC, 6 | n/d | n/d |
| 1000 °C, 36 h/MG | h-GaN, 100 | $a = 3.18$ | 25 (24–26) |
| | | $c = 5.18$ | |
| 1000 °C, 6 h/WBM | h-GaN, 100 | $a = 3.19$ | 21 (16–25) |
| | | $c = 5.19$ | |
| 1000 °C, 36 h/WBM | h-GaN, 99.7 | $a = 3.18$ | 24 (17–29) |
| | | $c = 5.18$ | |
| | W ₃ N ₄ , 0.2 | n/d | n/d |
| | W, 0.1 | n/d | n/d |
| 1100 °C, 36 h/MG | h-GaN, 100 | $a = 3.19$ | 48 (23–70) |
| | | $c = 5.18$ | |
| 1100 °C, 6 h/WBM | h-GaN, 99 | $a = 3.19$ | 41 (26–50) |
| | | $c = 5.19$ | |
| | W ₃ N ₄ , 0.8 | n/d | n/d |
| | W, 0.2 | n/d | n/d |
| 1100 °C, 36 h/WBM | h-GaN, 98.3 | $a = 3.19$ | 53 (47–62) |
| | | $c = 5.19$ | |
| | W ₃ N ₄ , 1.5 | n/d | n/d |
| | W, 0.2 | n/d | n/d |
| 1150 °C, 6 h/MG | h-GaN, 100 | $a = 3.19$ | 40 |
| | | $c = 5.19$ | |
| 1200 °C, 12 h/MG | Empty crucible – no product | | |

calculated and shown as a range of D of which spread can be linked to preferential crystal growth/crystal texturing.

Fig. 4 includes typical XRD patterns for nanopowders made from the ball milled GaP. In addition to the major h-GaN product, traces of contaminant c-W₃N₄ (JCPDS 75-1002) and elemental α -W (JCPDS 4-806) are also detected. Their occurrence can be explained by nitridation of the initially present WC with ammonia reported to take place above 900 °C; the resulting tungsten nitride is accompanied by elemental tungsten from nitride's decomposition under such conditions.²²

The content of Table 1 confirms the h-GaN as the only crystalline gallium nitride polytype formed under a broad range of applied conditions, *i.e.*, in the range 800–1150 °C and for all three ways of grinding. Complete nitridation was achieved after suitable reaction times at 900 °C and above whereas at 1200 °C/12 h no product was made due to GaN thermal instability (empty crucible). The average crystallite sizes ranged from 10 to a few tens of nanometers. For the highest nitridation temperatures, some crystallite texturing was evident as supported by varying D -values for different planes. The manually ground GaP

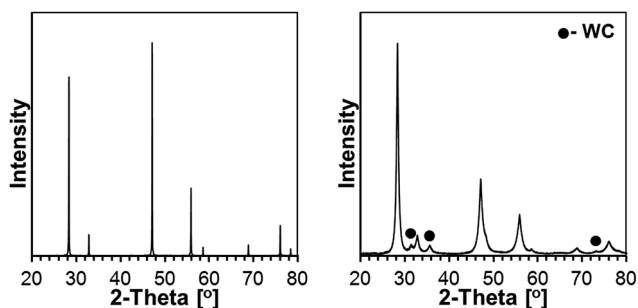


Fig. 2 XRD patterns for reference GaP substrates: left – manually ground, right – dry ball milled. Diffraction lines for adventitious hexagonal WC are shown with solid circles.

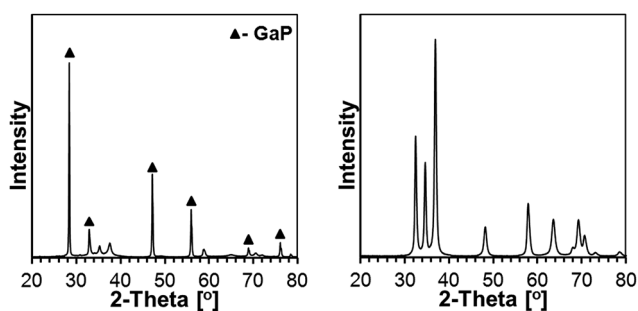


Fig. 3 Representative XRD patterns for GaN nanopowders prepared from manually ground GaP: left – 850 °C, 90 h; right – 900 °C, 60 h. GaP – solid triangles. Unmarked peaks are for h-GaN.

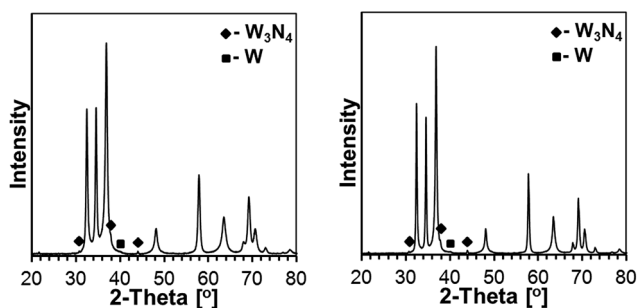


Fig. 4 Representative XRD patterns for GaN nanopowders prepared from wet ball milled GaP: left – 1000 °C, 36 h; right – 1100 °C, 36 h. W_3N_4 – solid diamonds, elemental α -W – solid squares. Unmarked peaks are for h-GaN.

afforded pure h-GaN powders whereas the ball milled GaP contained also small quantities of grinding ball-related impurities, *i.e.*, WC for temperatures <900 °C and W_3N_4 /W for temperatures >900 °C, independent on dry or wet milling conditions.

The representative SEM images of the manually ground reference GaP and the resulting GaN nanopowders are included in Fig. 5 in A and B, respectively. In the top row of B, the images for the 850 °C, 90 h-nitridation product are shown. Based on XRD data, this powder is composed of 26% of h-GaN and 74% of unreacted GaP supporting an incomplete whereas

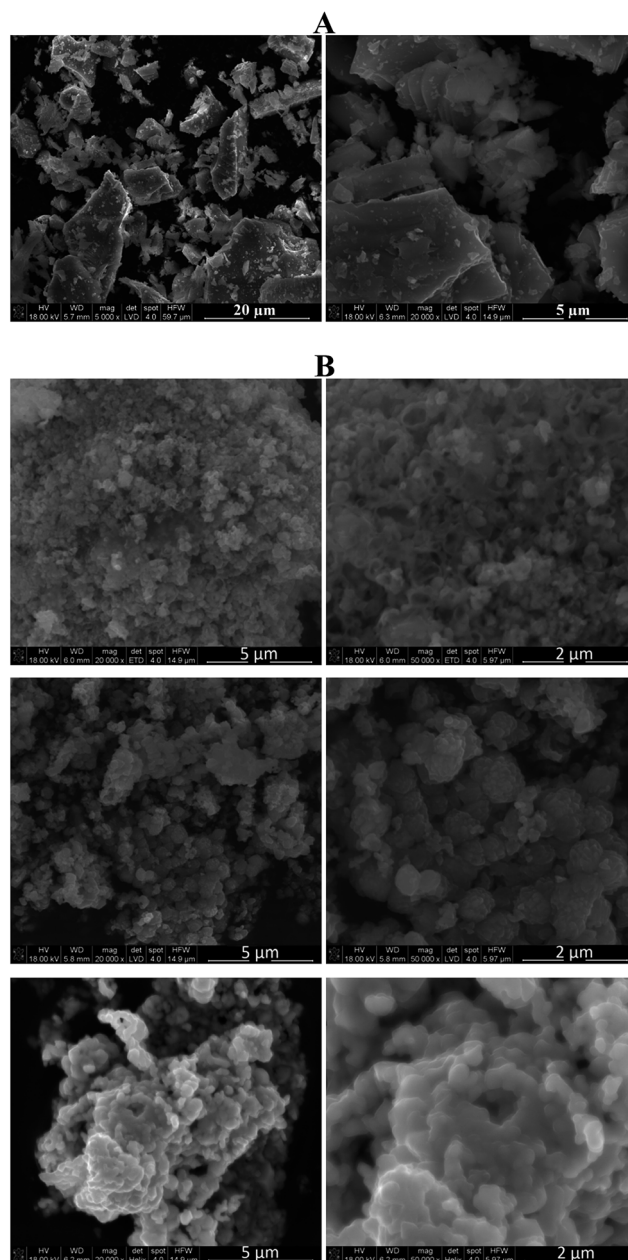


Fig. 5 SEM images of manually ground GaP and resulting GaN nanopowders: (A) – pure GaP; (B) – nitridation products: top row – 850 °C, 90 h; middle row – 1000 °C, 36 h; bottom row – 1100 °C, 36 h.

noticeable nitridation. Formation of thin-walled hollow spheres is consistent with progressing nitridation, likely, *via* reactions with NH_3 of molten Ga droplets from GaP decomposition. The images in the middle and bottom rows of B for complete nitridation support, again, an intermediate droplet formation by showing spheroidal hollow features/agglomerates with weakly bonded walls made of smaller nanocrystallites. It is instructive to compare particle size/shape evolution when going from the large microcrystalline pieces of ground GaP (A) to thin-walled hollow spheres of GaN in the partially nitrided product (B, top) to slightly agglomerated nonetheless regularly shaped GaN nanocrystallites from complete nitridation at the highest

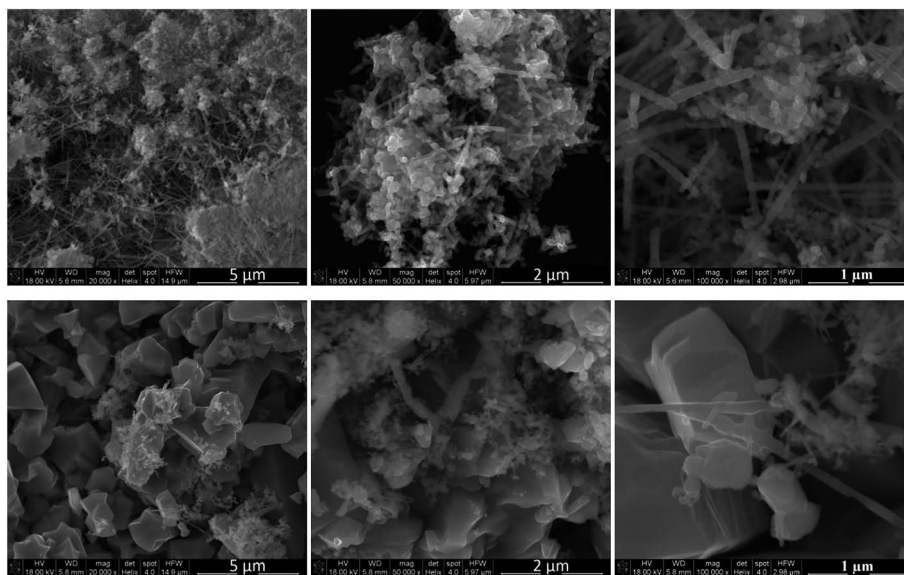


Fig. 6 SEM images of GaN nanopowders prepared from wet ball milled GaP: upper row – 1000 °C, 36 h; lower row – 1100 °C, 36 h.

temperature (B, bottom). It is to be noted that the observed grains are not necessarily crystallites but they rather represent crystallite agglomerates/aggregates or mixtures of the two types of particles.^{6f}

Distinctly different particle morphologies are displayed by GaN nanopowders made from the wet ball milled precursor, which are shown in Fig. 6. The 1000 °C, 36 h-powder is a mixture of several micrometer long tubercular nanowires with diameters of a few tens of nanometers and agglomerated lumps of quite regularly shaped nanoparticles with similar sizes (Fig. 6, upper row). The nanowires are manifestation of gas phase reactions possibly starting with sublimation of some GaP followed by reactions of the vapors with ammonia along the GaP + NH₃ pathway. The sublimation of the ball milled precursor is thought to be quite feasible and relatively efficient due to increased particle surface areas. A closer inspection of the middle image in the upper row shows that the numerous nanowires/nanorods tend to grow from nanoparticle seeds forming the lump. Consistently, the diameters of the nanowires are of the same dimension as the diameters of the nanoparticles. The origin of the regularly shaped and agglomerated particles in the lump could be linked to the decomposition of GaP with formation of gallium droplets that underwent nitridation along the Ga + NH₃ pathway. The liquid gallium seeds could have initiated growth of GaN nanowires fueled by the gas phase reactions as outlined above. One cannot exclude in nanowire growth, though, a catalytic effect of the contaminant tungsten in the ball milled materials. It needs to be stressed that all those samples showing by XRD some tungsten nitride and elemental tungsten (Table 1) did not show any tungsten in their SEM/EDX spectra acquired for many random areas and morphologies. This might mean that the scarce tungsten contaminant might have been just so finely distributed, such as in the tips of GaN nanorods, that was below detection limits of the EDX determinations. In this regard, the presence of metal

catalyst nanodroplets is frequently invoked in explaining 1D structures grown *via* the vapor–liquid–solid mechanism.

The 1100 °C, 36 h-powder has a distinctly different morphology compared with the lower temperature counterpart discussed above (Fig. 6, lower row). Most of it is made of large blocky crystallites whereas much smaller particle agglomerates and occasional thick rods are the minor features. Somewhat disappointedly, SEM/EDX shows no tungsten in any of the areas with various morphologies whereas XRD supports traces of tungsten nitride and elemental tungsten (*vide supra*). The presence of the minor fine habit is likely remnant of the similar habit seen as abundant in the 1000 °C, 36 h-powder, which apparently undergoes efficient recrystallization upon treatment at the higher temperature of 1100 °C. It is to recall that GaN nanopowder decomposition gradually wins the competition with recrystallization/crystal growth at 1000–1100 °C and higher.^{6h}

The UV-vis spectra determined for selected nanopowders also support the presence of hexagonal gallium nitride. The optical spectra (absorbance *vs.* wavelength) for a selected set of the 1000 °C and 1100 °C-nitrided samples are shown in Fig. 7 together with the Kubelka–Munk transformations, the latter enabling calculations of specific electronic transitions that are listed in Table 2. For gallium nitride materials, E_{g1} below *ca.* 3.0 eV corresponds likely to band tail transitions linked to various impurities, disorder, and defects and E_{g2} is related to the material's energy bandgap.²³ It is interesting to note that for bulk h-GaN, the bandgap transitions are expected at around $E_{g2(I)}$ equal to 3.4 eV whereas a shift to higher energies (blue shift) is expected for nanocrystallites with sizes below Bohr radius quoted to be in the range 3–11 nm.²⁴ The $E_{g2(II)}$ values at *ca.* 3.6–3.7 eV could be a manifestation of such a blue shift since the three nanopowders that display them may each contain a small crystallite fraction with sizes below 11 nm (Table 2). This can be estimated for two of them directly from the enclosed

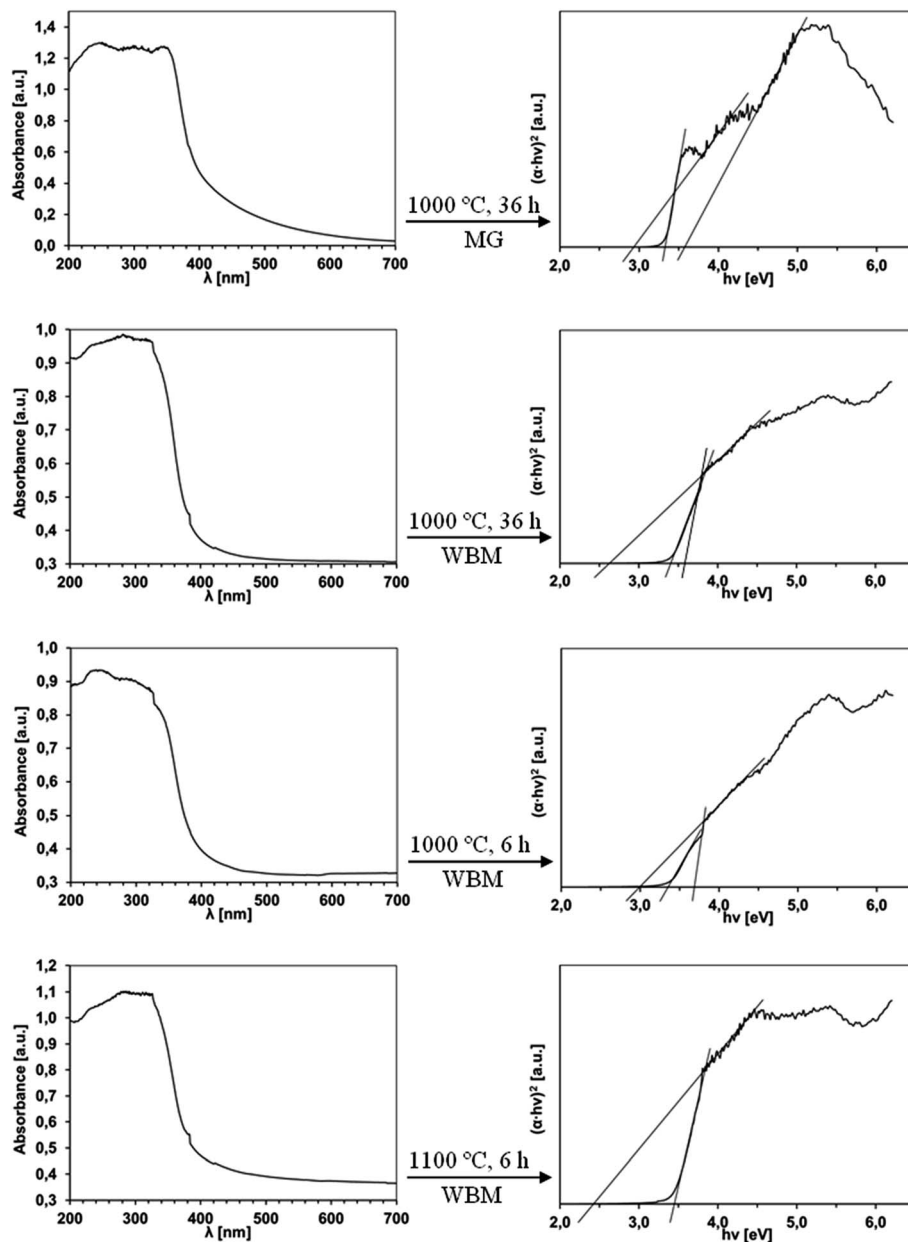


Fig. 7 Examples of UV-vis spectra of GaN from nitridation of ground GaP under indicated conditions. MG – manually ground, WBM – wet ball milled. The left panel shows original absorbance spectra whereas the right panel includes derived Kubelka–Munk functions.

Table 2 UV-vis derived E_g values of GaN nanopowders. MG – manual grinding, WBM – wet ball milling

| Nitridation | Grinding | E_{g1} [eV] | $E_{g2(I)}$ [eV] | $E_{g2(II)}$ [eV] |
|---------------|----------|---------------|------------------|-------------------|
| 1000 °C, 36 h | MG | 2.90 | 3.33 | 3.59 |
| 1000 °C, 36 h | WBM | 2.59 | 3.40 | 3.60 |
| 1000 °C, 6 h | WBM | 3.00 | 3.36 | 3.69 |
| 1100 °C, 6 h | WBM | 2.40 | 3.45 | — |

SEM pictures, *i.e.*, 1000 °C, 36 h, MG (Fig. 5) and 1000 °C, 36 h, WBM (Fig. 6). It is also evident that these two h-GaN samples that were made under identical conditions but from differently

ground GaP, differ also in their spectra stressing the underlying range of fine structural properties. In general terms, based on the UV-vis spectra the intrinsic nature of the completely nitrided samples appears to be quite diverse despite the matching XRD structures. This aspect will further be elaborated by the Raman and NMR studies.

Raman spectroscopy provides yet another insight into intrinsic structural properties of the nanopowders as a method being sensitive to chemical composition (purity), crystalline polytypes, and lattice defects/vacancies.²⁵ The micro-Raman spectra for selected samples are shown in Fig. 8 and the major peaks are listed in Table 3. For two samples from wet ball milling, D and E, that showed very strong luminescence, the spectra were acquired using a different laser source which

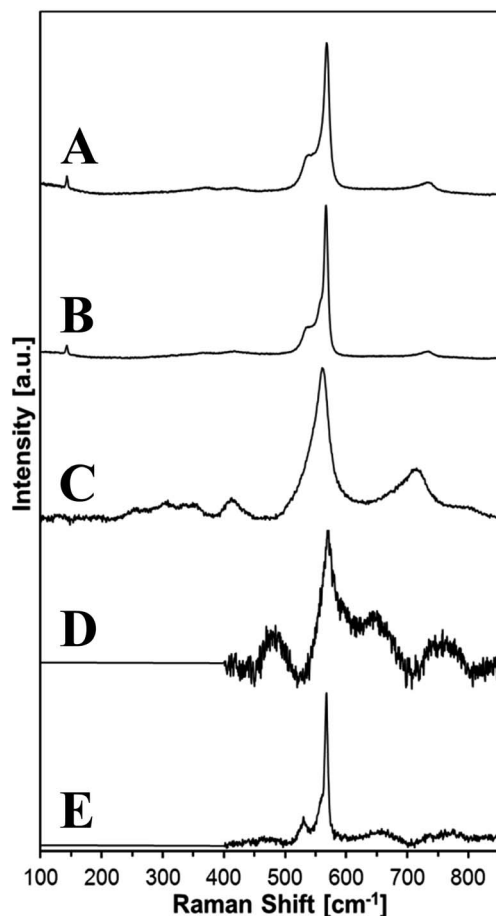


Fig. 8 Raman spectra of GaN nanopowders from nitridation of microcrystalline GaP. From top to bottom: (A) – 1000 °C, 36 h/MG; (B) – 1100 °C, 36 h/MG; (C) – 900 °C, 36 h/DBM; (D) – 1000 °C, 6 h/WBM; (E) – 1100 °C, 6 h/WBM. MG – manual grinding, DBM – dry ball milling, WBM – wet ball milling.

resulted in a narrower spectral range than otherwise recorded (see, Experimental). A precise origin of the non-specific emission is unknown but it could likely be linked to the W_3N_4/W impurities present in the two powders. All spectra were subjected to best-fitting deconvolution that yielded the peaks positions. In some cases of severe peak overlapping coupled with low intensities, e.g., in the range of 400 cm^{-1} and close to or above 700 cm^{-1} , the deconvolution might not have substantiated some weak and broad peaks that still could be present.

All phonon modes expected for hexagonal GaN, i.e., $A_1(\text{TO})$, $A_1(\text{LO})$, $E_1(\text{LO})$, $E_1(\text{TO})$, $E_2(\text{low})$, and $E_2(\text{high})$ are present in all spectra with the strongest mode of $E_2(\text{high})$ at $567\text{--}570\text{ cm}^{-1}$. The width of this mode can be used to analyze GaN lattice defects whereas the peak shift can be used to monitor residual stress in GaN thin films.²⁵ⁱ This peak is notably broadened for samples C and D implying structural inhomogeneities. In C, this is likely associated with low crystallinity/low nanosized particle range *via* a phonon confinement effect^{25a} whereas in D this can be due to two distinct morphologies (nanowires and lumps of regularly shaped nanocrystallites). A somewhat unexpected feature in all spectra is the presence of two weak and

broad peaks at *ca.* $300\text{--}360\text{ cm}^{-1}$ and *ca.* $410\text{--}480\text{ cm}^{-1}$ some of which are deconvoluted into two components. Literature interpretation of the peak above 300 cm^{-1} has involved either a lower symmetry activation of the otherwise silent $B_1(\text{low})$ mode in h-GaN^{25ef} or its assignment to the host lattice vibrational states^{25g} whereas the peak around 440 cm^{-1} has been proposed to result from nitrogen vacancy-related defects.^{25g} It is appropriate to mention that another weak peak at $646\text{--}670\text{ cm}^{-1}$ was also attributed to nitrogen defects^{25a,d,g} although $B_1(\text{high})$ activated mode was proposed as well.^{25f} Generally, the presence of the lattice-defect related peaks conforms well with the UV-vis results and ^{71}Ga MAS NMR data and the broad N-deficient phase peaks there (*vide infra*).

The spectra for the two samples made from the manually ground precursor, A and B, are remarkably similar to each other despite different synthesis temperatures and clearly differ from the remaining spectra, which stresses the importance of precursor grinding in GaN lattice evolution and quality. The peaks above *ca.* 800 cm^{-1} in samples C–E are tentatively assigned to tungsten-originated impurities. In this regard, the peak in C at 796 cm^{-1} (I) is in the region of W–C stretches in WC as determined by Raman spectroscopy.^{26a} The weak peaks (II) above 800 cm^{-1} in D and E could be linked to W–N stretches in the tungsten nitride impurity which is supported by the related W–C and W–O stretches^{26b,c} as well as by W–N stretches in some tungsten organometallic derivatives all seen in this region.^{26d}

A further insight into structural details of the nanopowders was gained with the solid state ^{71}Ga MAS NMR spectroscopy. The spectra of selected GaN nanopowders are shown in Fig. 9 and the peak positions are summarized in Table 4. We want to recall from our earlier NMR studies that hexagonal GaN may have two distinct gallium resonances, i.e., at *ca.* $325\text{--}330\text{ ppm}$ and *ca.* $415\text{--}440\text{ ppm}$.^{6h,i,27} The former peak is relatively sharp and corresponds to good uniformity of the short range structural order in well crystallized h-GaN whereas the latter lower field peak is significantly broadened. From the controversial literature data, the lower field peak has been assigned by some researchers either to a postulated N-deficient phase of GaN_{1-x} ($0 < x < 1$)²⁸ or from a different angle, alternatively, to a Knight shift due to the presence of conduction electrons in the semiconductor.²⁹ In our earlier studies, we observed an increased intensity of the lower field peak at the expense of the higher field peak for h-GaN nanopowders that were annealed at higher temperatures than the synthesis temperature. In our opinion, the temperature/time-induced nanopowder recrystallization, although results by XRD criteria in better crystallinity may, at the same time, introduce specific crystal defects including native N-defect formation and/or impurity oxygen incorporation into the regrown lattices.

The NMR spectra for the manually ground and wet ball milled reference GaP show a single resonance at 307 ppm in both cases (Fig. 9, left panel) agreeing well with literature data.³⁰ The set of spinning side bands is an artefact of the 6 kHz probe spinning. The spectrum for the manually ground sample is sharp and quite symmetrical indicating no significant second order quadrupolar interactions, which is expected for the cubic lattice of GaP. The spectrum for the wet ball milled sample is clearly broader and asymmetrical and this can indirectly be

Table 3 Positions of deconvoluted peaks in micro-Raman scattering determinations for GaN nanopowders. Labels A–E are the same as in Fig. 8. MG – manual grinding, DBM – dry ball milling, WBM – wet ball milling

| Mode assignment | Raman shift [cm^{-1}] | | | | |
|---|----------------------------------|---------------|--------------|--------------|--------------|
| | MG | | DBM | WBM | |
| | 1000 °C, 36 h | 1100 °C, 36 h | 900 °C, 36 h | 1000 °C, 6 h | 1100 °C, 6 h |
| | A | B | C | D | E |
| $E_2(\text{low})^{25a-d}$ | 143 | 143 | — | X | |
| Zone boundary, ^{25a} WC impurity | | | 260 | | |
| $B_1(\text{low})$ silent, ^{25e,f} lattice vibrations ^{25g} | 360 | 357 | 304 348 | | |
| N-vacancies, ^{25g} zone boundary ^{25a} | 418 | 426 | 413 | 411 482 | 467 |
| $A_1(\text{TO})^{25a-d}$ | 536 | 537 | 540 | — | 530 |
| $E_1(\text{LO})^{25a-d}$ | 560 | 560 | 562 | — | 559 |
| $E_2(\text{high})^{25a-d}$ | 568 | 567 | — | 570 | 567 |
| $B_1(\text{high})$ silent, ^{25f} defect induced vacancies, ^{25a,d,g} free carriers ^{25h} | 659 | 650 | 600 670 | 598 646 | 651 |
| $A_1(\text{LO}), E_1(\text{TO})^{25a}$ | 730 | 729 | 714 | 735 765 | 733 768 |
| WC (I) ^{26a} W_3N_4 (II) ^{26b,c} | | | 796 (I) | 844 (II) | 835 (II) |

accounted for by some degree of material amorphization upon milling associated with increased particle surface area – the surface atoms are under a different and lower symmetry

environment than in bulk and, thus, quadrupolar interactions may come to play.

The spectrum for the 850 °C, 150 h-sample confirms only partial nitridation, as substantiated also by XRD, and shows the prevailing peak at 307 ppm for unreacted GaP. The much weaker peak at *ca.* 325 ppm corresponds well with the expected high field peak for h-GaN while a potential low field peak at *ca.* 415 ppm is either too weak to be discernible or absent at all. It is worth to note that there is no evidence for any other peak, any other Ga-bearing species such as a mixed pnictide GaPN. All spectra for the completely nitrated materials have both peaks expected for h-GaN (Fig. 9, right panel).

When comparing the data for the powders made at 1000 °C, 6 h and 1000 °C, 36 h it is apparent that they have virtually the same features, namely, the prevailing high field resonance at 326 ppm and the weaker and much broader resonance at 415 ppm. It means that the extension of conversion time from 6 to 36 hours at the same temperature was insignificant from the point of view of the nitride's close range order features. The long range order probed by XRD for these two samples is very much alike, too, as judged by both the cell parameters and average crystallite sizes (Table 1). Also, the general appearance of the UV-vis spectra for these samples is similar and the derived bandgap values $E_{g2}(\text{I})$ and $E_{g2}(\text{II})$ are very close to each other whereas there is some difference in the band tail transitions at energies lower than 3 eV (Fig. 7, Table 2). Since the latter are linked to some specific lattice disorder and defects, the difference reflects the impact of nitridation time on this property.

A significant change in the NMR spectra takes place upon increasing the nitridation temperature from 1000 to 1100 °C,

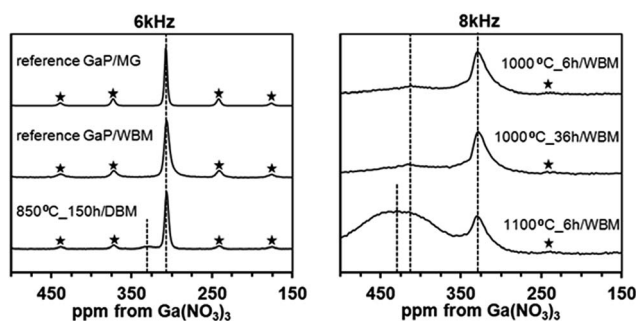


Fig. 9 Solid state ^{71}Ga MAS NMR spectra of GaP (reference) and GaN nanopowders from nitridation of GaP. MG – manually ground, DBM – dry ball milled, WBM – wet ball milled. Left panel – 6 kHz probe spinning rate, right panel – 8 kHz probe spinning rate. Asterisks indicate spinning side bands.

Table 4 ^{71}Ga MAS NMR peak positions for selected nanopowders. MG – manual grinding, DBM – dry ball milling, WBM – wet ball milling

| Nitridation | Grinding | High field peak [ppm] | Low field peak [ppm] |
|---------------|----------|-----------------------|----------------------|
| 850 °C, 150 h | DBM | 325 | — |
| 1000 °C, 6 h | WBM | 326 | 415 |
| 1000 °C, 36 h | WBM | 326 | 415 |
| 1100 °C, 6 h | WBM | 328 | 430 |

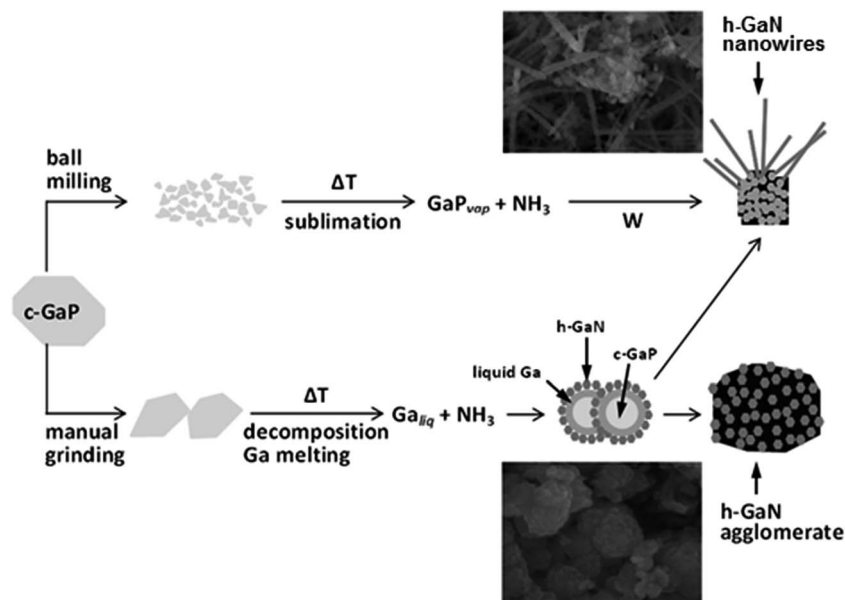


Fig. 10 Ammonolytical nitridation of microcrystalline particles of c-GaP to nanocrystalline particles of h-GaN of various habits.

which is clearly seen when comparing two spectra for the relevant powders after the 6 h-nitridation time (Fig. 9, right panel). The broad peak at *ca.* 430 ppm becomes predominant pointing out to a prevalingly “defected” short range order in this powder. This temperature effect is consistent with what we observed for numerous GaN nanopowders in our previous studies^{6h,i,27} as well with the outcome for the system GaSb/NH₃^{10d} when annealing under NH₃ at higher temperatures resulted in relatively higher intensities of the 430 ppm peak. On the one hand, higher nitridation/annealing temperatures usually yield better crystallinity by XRD (mainly, due to recrystallization/crystal growth) but, on the other hand, this is accompanied by higher N-native and/or impurity oxygen defect proportions.

It is evident that only the combination of various methods such as XRD diffractometry and UV-vis, Raman, and NMR spectroscopies can provide a comprehensive description of the nanopowder structures with diverse intrinsic properties. A challenging task is still ahead to correlate the methods various information/parameters with definite structural details. In this regard, the application of high resolution TEM may in favorable cases be useful but such an approach was outside the scope of this project. In the domain of research on gallium nitride, undoubtedly, there is also an urgent need for developing sensitive analytical methods for unequivocal determination of structural defects including N-native defects and O-impurities.

3.3. Pathways in ammonolysis of microcrystalline GaSb

A conceptual picture that emerges from this study is consistent with a characteristic reactivity pattern in the ammonolysis of bulk microcrystalline GaP, which includes two distinct pathways both resulting in nanopowders of the thermodynamically stable hexagonal GaN. Depending on circumstances, one pathway seems to lead to h-GaN *via* ammonolysis of molten Ga droplets from decomposed GaP whereas another involves gas phase

ammonolysis reactions of sublimed GaP species. The first pathway is specific for relatively large GaP particles such as those from manual grinding whereas the second pathway is activated for much finer GaP particles with increased surface area from ball milling. Fig. 10 illustrates the proposed sequence of major events for both pathways supported by the experimental data.

Specifically, the data confirm the exclusive formation of h-GaN and, therefore, point out to a negligible role of a transient cubic GaPN and its potential conversion to c-GaN in contrast to the related systems of GaAs/NH₃ and GaSb/NH₃. In the initial nitridation stages at sufficiently high temperatures of 900–1150 °C and for large particles, it is rather the thermally driven decomposition of GaP winning the competition against sublimation and resulting first in thin liquid gallium layers on substrate particles. Then, the *in statu nascendi* gallium efficiently reacts with ammonia towards the stable h-GaN along $\text{Ga}_{\text{liq}} + \text{NH}_3 \rightarrow \text{GaN} + 3/2\text{H}_2$. For much smaller particles with increased surface area the GaP sublimation prevails creating advantageous conditions for gas phase reactions summarized by $\text{GaP}_{\text{vap}} + \text{NH}_3 \rightarrow \text{GaN} + \text{PH}_3$ with the predominant formation of h-GaN nanowires/nanorods. A detailed mechanism of nanowire formation may involve catalytic action of adventitious tungsten species from milling ball attrition. This aspect requires suitably focused further studies which are beyond the scope of the current project. Also, it appears that the overall long nitridation times in the studied temperature range, especially at 900 °C, are determined rather by a relatively slow decomposition and sublimation of GaP than by the by-products volatility/removal.

4. Conclusions

The ammonolytical nitridation of GaP is a convenient way for a one-stage preparation of hexagonal GaN nanopowders of high purity, very good crystallinity, and diverse morphologies

including the regularly shaped particles and/or 1D nanowire/nanorod structures. The exclusive formation of the stable h-GaN polytype under a wide range of experimental conditions and the substrate's particle sizes points out to reaction pathways favoring the thermodynamically determined product. These pathways are proposed to include reactions of ammonia with metallic Ga from GaP decomposition or with sublimed GaP species. The potential topochemically-controlled pnitide-metathesis reaction *via* substitution of P-centers in the cubic GaP with N-centers from ammonia, which could yield the metastable cubic GaN, is not detected at all. This is in contrast to the related systems of GaAs/NH₃ and GaSb/NH₃ where both GaN polytypes were shown to form under comparable conditions. The ammonolysis of GaP, combined with the previously published studies on the two related systems, enables now control over making a wide range of GaN polytype mixtures including a pure hexagonal variety, average particle sizes, morphologies, and structural integrity. A challenging question remains open, however, as to tuning any of these systems to make pure cubic GaN.

Acknowledgements

The study was supported by the National Science Center (NCN) in Poland, Grant No. 2013/09/B/ST5/01223.

References

- (a) I. Akasaki, *Angew. Chem., Int. Ed.*, 2015, **54**(17), 7750–7763; (b) H. Amano, *Angew. Chem., Int. Ed.*, 2015, **54**(17), 7764–7769; (c) S. Nakamura, *Angew. Chem., Int. Ed.*, 2015, **54**(17), 7770–7788; (d) H. P. Maruska and W. C. Rhines, *Solid-State Electron.*, 2015, **111**, 32–41; (e) S. S. Khludkov, I. A. Prudaev and O. P. Tolbanov, *Russ. Phys. J.*, 2013, **55**, 903–909; (f) M. S. Kang, C. H. Lee, J. B. Park, H. Yoo and G. C. Yi, *Nano Energy*, 2012, **1**, 391–400.
- (a) T. Hashimoto, E. Letts and S. Hoff, *Sens. Mater.*, 2013, **25**, 155–164; (b) R. Dwilinski, R. Doradzinski, J. Garczynski, L. Sierzputowski, R. Kucharski, M. Zajac, M. Rudzinski, R. Kudrawiec, W. Strupinski and J. Misiewicz, *Phys. Status Solidi A*, 2011, **208**, 1489–1493; (c) M. Bockowski, P. Strak, I. Grzegory and S. Porowski, *Technology of gallium nitride crystal growth*, *Book Series: Springer Series in Materials Science*, 2010, vol. 133, pp. 207–234; (d) V. Avrutin, D. Silversmith, Y. Mori, F. Kawamura, Y. Kitaoka and H. Morkoc, *Proc. IEEE*, 2010, **98**, 1302–1315.
- (a) T. Dietl and H. Ohno, *Rev. Mod. Phys.*, 2014, **86**, 187–252; (b) T. Jungwirth, J. Wunderlich, V. Novak, K. Olejnik, B. L. Gallagher, R. P. Campion, K. W. Edmonds, A. W. Rushforth, A. J. Ferguson and P. Nemeč, *Rev. Mod. Phys.*, 2014, **86**, 855–896; (c) A. Hirohata and K. Takanashi, *J. Phys. D: Appl. Phys.*, 2014, **47**, 193001; (d) K. Varaprasad, K. Ramam, G. S. M. Reddy and R. Sadiku, *RSC Adv.*, 2014, **4**, 60363–60370; (e) M. Drygas, J. F. Janik, M. M. Bucko, J. Gosk and A. Twardowski, *RSC Adv.*, 2015, **5**, 37298–37313.
- (a) M. A. Malik, M. Afzaal and P. O'Brien, *Chem. Rev.*, 2010, **110**, 4417–4446; (b) B. Mazumder and A. L. Hector, *J. Mater. Chem.*, 2009, **19**, 4673–4686; (c) C. N. R. Rao, C. R. C. Vivekchand, K. Biswas and A. Govindaraj, *Dalton Trans.*, 2007, 3728–3749; (d) J. A. Jegier, S. McKernan, A. P. Purdy and W. L. Gladfelter, *Chem. Mater.*, 2000, **12**, 1003–1010.
- R. L. Wells and J. F. Janik, *Eur. J. Solid State Inorg. Chem.*, 1996, **33**, 1079–1090.
- (a) J. F. Janik and R. L. Wells, *Chem. Mater.*, 1996, **8**, 2708–2711; (b) J. L. Coffey, M. A. Johnson, L. Zhang, R. L. Wells and J. F. Janik, *Chem. Mater.*, 1997, **9**, 2671–2673; (c) J. F. Janik, R. L. Wells, J. L. Coffey, J. V. St John, W. T. Pennington and G. L. Shimek, *Chem. Mater.*, 1998, **10**, 1613–1622; (d) J. L. Coffey, T. W. Zerda, R. Appel, R. L. Wells and J. F. Janik, *Chem. Mater.*, 1999, **11**, 20–22; (e) L. Czepirski, J. F. Janik, E. Komorowska-Czepirska and R. L. Wells, *Adsorpt. Sci. Technol.*, 2002, **20**, 723–728; (f) R. L. Jouet, A. P. Purdy, R. L. Wells and J. F. Janik, *J. Cluster Sci.*, 2002, **13**, 469–486; (g) J. F. Janik, *Powder Technol.*, 2005, **152**, 118–126; (h) M. Drygas, Z. Olejniczak, E. Grzanka, M. M. Bucko, R. T. Paine and J. F. Janik, *Chem. Mater.*, 2008, **20**, 6816–6828; (i) M. Drygas and J. F. Janik, *Mater. Chem. Phys.*, 2012, **133**, 932–940.
- J. F. Janik and R. L. Wells, *Inorg. Chem.*, 1997, **36**, 4135–4137.
- (a) G. L. Wood, E. A. Pruss and R. T. Paine, *Chem. Mater.*, 2001, **13**, 12–14; (b) J. F. Janik, M. Drygas, S. Stelmakh, E. Grzanka, B. Palosz and R. T. Paine, *Phys. Status Solidi A*, 2006, **203**, 1301–1306.
- (a) S. Stelmakh, A. Swiderska-Sroda, G. Kalisz, S. Gierlotka, E. Grzanka, B. Palosz, M. Drygas, J. F. Janik and R. T. Paine, *Proceedings of the International Conference on Nanoscience and Technology*, Basel, Switzerland, July 30–Aug 4, 2006, Institute of Physics Publishing, Philadelphia, PA, 2006; (b) E. Grzanka, S. Stelmakh, S. Gierlotka, A. Swiderska-Sroda, G. Kalisz, B. Palosz, M. Drygas, J. F. Janik and R. T. Paine, *European Powder Diffraction Conference, EPDIC-10*, Geneva, Switzerland, Sept. 1–4, 2006, *Z. Kristallogr.*, 2007, **26**, MS11; (c) J. Borysiuk, P. Caban, W. Strupinski, S. Gierlotka, S. Stelmakh and J. F. Janik, *Cryst. Res. Technol.*, 2007, **42**, 1291–1296; (d) J. F. Janik, M. Drygas, C. Czosnek, B. Palosz, S. Gierlotka, S. Stelmakh, E. Grzanka, G. Kalisz, A. Świdarska-Środa, M. Leszczyński, G. Nowak and R. Czernecki, *Way to make sintered gallium nitride GaN*, No. 2/2012, Polish patent No. P-378458, 29 February 2012.
- (a) A. Addamiano, *J. Electrochem. Soc.*, 1961, **108**, 1072–1072; (b) W. S. Jung, O. H. Han and S. A. Chae, *Mater. Chem. Phys.*, 2006, **100**, 199–202; (c) M. Drygas, M. M. Bucko, E. Grzanka and J. F. Janik, *Curr. Nanosci.*, 2013, **9**, 173–182; (d) M. Drygas, P. Jelen, M. M. Bucko, Z. Olejniczak and J. F. Janik, *RSC Adv.*, 2015, **5**, 82576–82586.
- (a) R. Chow and Y. G. Chai, *J. Vac. Sci. Technol.*, A, 1983, **1**, 49–54; (b) A. S. Jordan and A. Robertson, *J. Vac. Sci. Technol.*, A, 1994, **12**, 204–215; (c) K. Lodders, *J. Phys. Chem. Ref. Data*, 1999, **28**, 1705–1712; (d) S. L. Wright and H. Kroemer, *J. Vac. Sci. Technol.*, 1982, **20**, 143–148.
- (a) C. D. Thurmond, *J. Phys. Chem. Solids*, 1965, **26**, 785–802; (b) V. B. Ufimtsev, V. P. Shumilin, A. N. Krestovnikov and

- V. N. Vigdorovich, *Russ. J. Phys. Chem.*, 1970, **44**, 624–625; (c) H. W. Seo, S. Y. Bae, J. Park, H. Yang and S. Kim, *Chem. Commun.*, 2002, 2564–2565.
- 13 (a) S. Ratanathammaphan, S. Thainoi, P. Changmoang, S. Sopitpan and C. Antarasena, *J. Cryst. Growth*, 2001, **227–228**, 260–265; (b) M. J. Mondry, E. J. Caine and H. Kroemer, *J. Vac. Sci. Technol.*, A, 1985, **3**, 316–318.
- 14 (a) H. W. Seo, S. Y. Bae, J. Park, M. Kang and S. Kim, *Chem. Phys. Lett.*, 2003, **378**, 420–424; (b) H. M. Kim, S. Hayashi and K. Yamamoto, *J. Phys.: Condens. Matter*, 1996, **8**, 2705–2714; (c) B. Gil, J. P. Albert, J. Casmassel, H. Mathieu and C. Benoit à la Guillaume, *Phys. Rev. B: Condens. Matter Mater. Phys.*, 1986, **33**, 2701–2712; (d) V. K. Bazhenov and V. I. Fistul, *Soviet Physics–Semiconductors*, 1984, **18**, 843–853.
- 15 (a) G. Lidgard, R. Nicklin and P. B. Hart, *J. Phys. D: Appl. Phys.*, 1973, **6**, L75–L79; (b) J. I. Pankove, *Optical Processes in Semiconductors*, Dover Publ., New York, 1971.
- 16 S. M. Gao, L. Y. Zhu, Y. Xie and X. B. Qian, *Eur. J. Inorg. Chem.*, 2004, 557–561.
- 17 (a) C. Y. Yeh, Z. W. Lu, S. Froyen and A. Zunger, *Phys. Rev. B: Condens. Matter Mater. Phys.*, 1992, **46**, 10086; (b) A. Zoroddu, F. Bernardini, P. Ruggerone and V. Fiorentini, *Phys. Rev. B: Condens. Matter Mater. Phys.*, 2001, **64**, 045208.
- 18 S. V. Novikov, N. M. Stanton, R. P. Champion, C. T. Foxon and A. J. Kent, *J. Cryst. Growth*, 2008, **310**, 3964–3967.
- 19 (a) A. P. Purdy, R. J. Jouet and C. F. George, *Cryst. Growth Des.*, 2002, **2**, 141–145; (b) W. Y. Wang, Y. P. Xu, D. F. Zhang and X. L. Chen, *Mater. Res. Bull.*, 2001, **36**, 2155–2162.
- 20 (a) B. W. Jacobs, V. M. Ayres, M. P. Petkov, J. B. Halpern, M. He, A. D. Baczewski, K. McElroy, M. A. Crimp, J. M. Zhang and H. C. Shaw, *Nano Lett.*, 2007, **7**, 1435–1438; (b) S. Suandon, S. Sanorpim, K. Yoodee and K. Onabe, *Thin Solid Films*, 2007, **515**, 4393–4396; (c) B. W. Jacobs, V. M. Ayres, M. A. Crimp and K. McElroy, *Nanotechnology*, 2008, **19**, 405706; (d) S. V. Cherepanova, *J. Struct. Chem.*, 2012, **53**, S109–S132.
- 21 (a) C. Y. Yeh, Z. W. Lu, S. Froyen and A. Zunger, *Phys. Rev. B: Condens. Matter Mater. Phys.*, 1992, **46**, 10086–10097; (b) A. Zoroddu, F. Bernardini, P. Ruggerone and V. Fiorentini, *Phys. Rev. B: Condens. Matter Mater. Phys.*, 2001, **64**, 045208.
- 22 X. S. Zhou, Y. J. Qiu, J. Yu, J. Yin and S. Gao, *Int. J. Hydrogen Energy*, 2011, **36**, 7398–7404.
- 23 I. Akyuz, S. Kose, F. Atay and V. Bilgin, *Semicond. Sci. Technol.*, 2006, **21**, 1620–1626.
- 24 (a) P. Ramvall, S. Tanaka, S. Nomura, P. Riblet and Y. Aoyagi, *Appl. Phys. Lett.*, 1998, **73**, 1104–1106; (b) X. L. Chen, J. N. Li, Y. G. Cao, Y. C. Lan, H. Li, M. He, C. Y. Wang, Z. Zhang and Z. Y. Qiao, *Adv. Mater.*, 2000, **12**, 1432–1434.
- 25 (a) M. Gopalakrishnan, V. Purushothaman, P. S. Venkatesh, V. Ramakrishnan and K. Jeganathan, *Mater. Res. Bull.*, 2012, **47**, 3323–3329; (b) Y. S. Wu, W. K. Chang and H. Y. Lai, *J. Cryst. Growth*, 2008, **310**, 2800–2805; (c) M. S. Kumar and J. Kumar, *Mater. Chem. Phys.*, 2002, **77**, 341–345; (d) H. Harima, *J. Phys.: Condens. Matter*, 2002, **14**, R967–R993; (e) A. Hushur, M. H. Manghnani and J. Narayan, *J. Appl. Phys.*, 2009, **106**, 054317; (f) F. J. Manjóna, B. Mari, J. Serrano and A. H. Romero, *J. Appl. Phys.*, 2005, **97**, 053516; (g) M. Katsikini, K. Papagelis, E. C. Paloura and S. Ves, *J. Appl. Phys.*, 2003, **94**, 4389–4394; (h) A. Kaschner, A. Hoffmann, C. Thomse, F. Bertram, T. Riemann, J. Christ, K. Hiramatsu, H. Sone and N. Sawak, *Appl. Phys. Lett.*, 2000, **76**, 3418–3420; (i) L. T. Tung, K. L. Lin, E. Y. Chang, W. C. Huang, Y. L. Hsiao and C. H. Chiang, *J. Phys.: Conf. Ser.*, 2009, **187**, 012021.
- 26 (a) B. Q. Yang, X. P. Wang, H. X. Zhang, Z. B. Wang and P. X. Feng, *Mater. Lett.*, 2008, **62**, 1547–1550; (b) J. H. Kim and K. L. Kim, *Appl. Catal.*, A, 1999, **181**, 103–111; (c) A. Baserga, V. Russo, F. Di Fonzo, A. Bailini, D. Cattaneo, C. S. Casari, A. Li Bassi and C. E. Bottani, *Thin Solid Films*, 2007, **515**, 6465–6469; (d) Z. J. Tonzetich, R. R. Schrock, K. M. Wampler, B. C. Bailey, C. C. Cummins and P. Mülle, *Inorg. Chem.*, 2008, **47**, 1560–1567.
- 27 M. Drygas, M. M. Bucko, Z. Olejniczak, I. Grzegory and J. F. Janik, *Mater. Chem. Phys.*, 2010, **122**, 537–543.
- 28 (a) W. S. Jung, C. Park and S. Han, *Bull. Korean Chem. Soc.*, 2003, **24**, 1011–1013; (b) W. S. Jung, *Mater. Lett.*, 2006, **60**, 2954–2957; (c) W. S. Jung, O. H. Han and S. A. Chae, *Mater. Chem. Phys.*, 2006, **100**, 199–202; (d) B. Schwenzer, J. Hu, R. Seshadri, S. Keller, S. P. DenBaars and U. K. Mishra, *Chem. Mater.*, 2004, **16**, 5088–5095; (e) B. Schwenzer, J. Hu, Y. Wu and U. K. Mishra, *Solid State Sci.*, 2006, **8**, 1193–1201.
- 29 (a) J. P. Yesinowski and A. P. Purdy, *J. Am. Chem. Soc.*, 2004, **126**, 9166–9167; (b) J. P. Yesinowski and A. P. Purdy, *J. Am. Chem. Soc.*, 2006, **128**, 4952–4953; (c) J. P. Yesinowski, *Phys. Status Solidi C*, 2005, **2**, 2399–2402; (d) J. P. Yesinowski, in *Solid State NMR Book Series Topics in Current Chemistry*, ed. J. C. C. Chan, Springer, 2012, vol. 306, ch. Solid-state NMR of inorganic semiconductors, pp. 229–312.
- 30 O. H. Han, H. K. C. Timken and E. Oldfield, *J. Chem. Phys.*, 1988, **89**, 6046–6052.